Engineering and Applied Sciences
2017; 2(5): 89-98
http://www.sciencepublishinggroup.com/j/eas
doi: 10.11648/j.eas.20170205.12
ISSN: 2575-2022 (Print); ISSN: 2575-1468 (Online)

Comparative Analysis Between *Cam* and *Cam-less* Valve Actuating for Automotive System

Aliyu Bhar Kisabo, Musa James Ibrahim, Opasina Ayodele Oluwafemi

Centre for Space Transport & Propulsion (CSTP) Epe, Lagos, Nigeria

Email address:
aliyukisabo@yahoo.com (A. B. Kisabo), jamescap02@yahoo.com (M. J. Ibrahim), ayodeleopasina@yahoo.com (O. A. Opasina)

To cite this article:
Aliyu Bhar Kisabo, Musa James Ibrahim, Opasina Ayodele Oluwafemi. Comparative Analysis Between *Cam* and *Cam-less* Valve Actuating for Automotive System. *Engineering and Applied Sciences*. Vol. 2, No. 5, 2017, pp. 89-98. doi: 10.11648/j.eas.20170205.12

Received: March 15, 2017; **Accepted**: April 17, 2017; **Published**: November 28, 2017

Abstract: A promising alternative of the conventional camshaft in *internal combustion* engines is one that replaces the camshaft with electromagnetic actuators. This so-called *camless* system provides great opportunities for the automotive industry. To investigate the advantage of the system against the cam system firstly, we modelled the lift profiles of both systems with novel mathematical expressions. For the *camless* system we modelled an Electromagnetic Valve Actuating (EMVA) system that captures a plant transfer function and a PID controller with a set-point tracking scheme. Simulation result in MATLAB/Simulink of the theoretical *camless* lift profile was imported into Curve Fitting (CF) Toolbox of MATLAB and the novel mathematical model was realized. Experimentally measured data for the *camless* lift profile were then fitted with this model and a *tuned* experimental model was realized. While for the cam system, the mathematical model was developed directly from experimental data via Curve Fitting Toolbox of MATLAB. Secondly, we computed volumetric efficiencies of both systems using the novel mathematical lift profiles at different engine speeds. The *camless* system was observed to outperform the cam system.

Keywords: Camless System (EMVA), Cam System, MATLAB/Simulink, Curve Fitting Toolbox

1. Introduction

The opening and closing phase of exhaust and intake valves of current automotive engines use mechanical driven camshaft. Thus, the lift profile of such valves depends on the crankshaft position [1, 2]. This implies that the valve train is not a flexible; once the cam-follower mechanism is designed during the engine development, it is not possible to adapt in real time the valve features according to the engine working conditions, over the entire range of speed.

To meet the expectations of current and future customers, new internal combustion engines must be fuel economical and more efficient [3, 4, 5, 6, 7].

An attempt to modify the cam system to be more efficient was restricted from the fact that at high speed, engine performance deteriorates and valves do not evolve in a regular periodic motion [8].

Thus, internal combustion engines evolution is pointing towards the more promising cam-less (without a cam) solution [9]. Here, the conventional cam in the traditional internal combustion engines is replaced with a single actuator to drive each valve. Of such engines, is one that the valve actuation is conducted by a combination of electrical and magnetic (electro-magnetic) forces.

1.1. Electro-Magnetic Valve Actuating System (EMVA)

A typical EMVA is referred to as a cam-less system consists primarily of two opposite permanent magnets and two balanced springs working in parallel [10].

In this study, the camless system architecture considered for a camless internal combustion engine is presented in figure 1. The current flow in this arrangement is in the same direction (causing an equal push-pull electromotive force on the armature during the valve stroke) due to the fact that the upper and lower coils are connected in series. This arrangement also helps in eliminating *back-electromotive force* during the system operation. The EMVA consists of stationary permanent magnets, stationary copper coils, and a moving armature made of steel, on which the valve is rigidly attached. Thus, a bi-directional force is being transmitted to the valve. When there is no electric current, the armature rests in a position that causes the valve to be closed. The two balanced springs and

permanent magnets help to achieve this gas tight seal during compression. Note that the same force that causes the valve closing also causes the valve opening, implying that both coils are of the same spring constant and length [11].

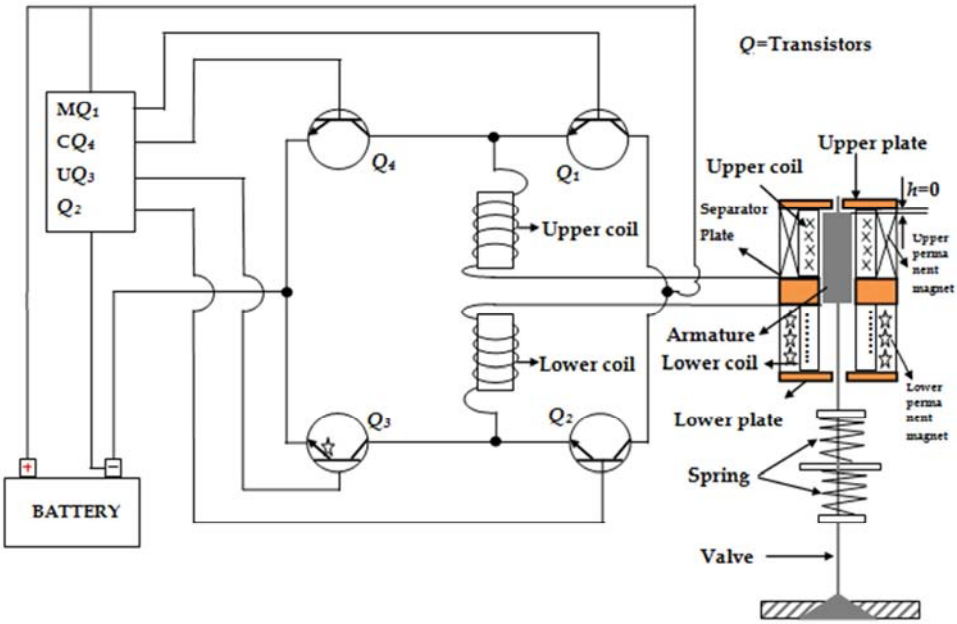

Figure 1. *Schematic of the camless system.*

Essentially in figure 1, there are two magnetic circuits, one with permanent magnets and one with electromagnetic coils.

An H-bridge electronic circuit that enables voltage to be applied across the actuator in either direction ensured the movement of the actuator. The H-bridge is built with four power transistors (Q_1, Q_2, Q_3, and Q_4) which serve as switches as well as current regulators. When the power transistor Q_1, and $Q_3$are closed (and Q_2, and Q_4 are open) a positive voltage will be applied across the actuator. By opening Q_1, and Q_3 closing Q_2, and Q_4, this voltage is reversed, allowing reverse operation of the actuator [12].

Despite its apparent simplicity, the behaviour of this camless system is affected by many nonlinear phenomena which can dramatically alter its dynamics, some of which are;

a. Friction, including all friction forces along all the sliding parts.
b. Impacts, occurring when one of the moving bodies in the system (valve, armature) hits mechanical constraints [13, 14].

Thus, the EMVA system is a sandwich of mechanical and electrical elements working together. These elements need to be isolated during studies like this in an attempt to understand its dynamics.

1.2. Camless Sub-systems

The camless system comprises of various subsystem that interact, these are; electrical, magnetic, gaseous and mechanical subsystems. A mass-spring-damper is use to represent the mechanical subsystem of the camless system as shown in figure 2 (b) [15]. The mass m [kg] in figure 2(b) is the combined masses of the armature and the valve. In figure 2(a), h is the distance between the armature and the upper plate, $h \in (0,8)$.

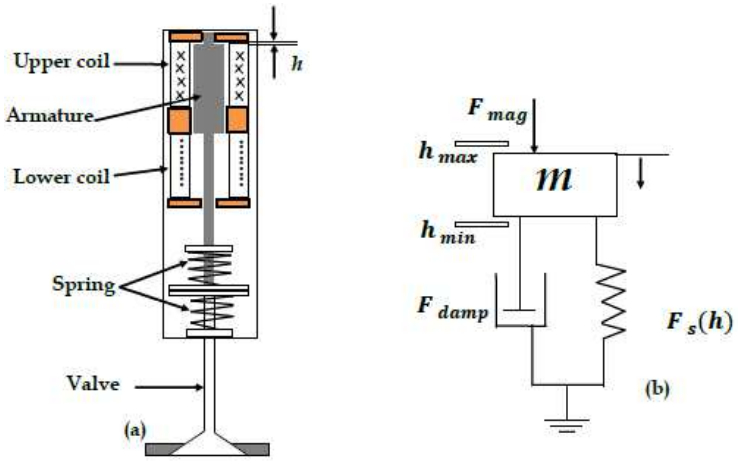

Figure 2. *The mechanical camless subsystem: (a) schematic of mechanical subsystem; (b) mass-spring damper representing the camless system.*

2. Mathematical Model of the Camless System

A free-body-diagram of the forces acting on the valve is shown in Fig. 3. Downwards and upward positions of forces are considered as negative and positive respectively.

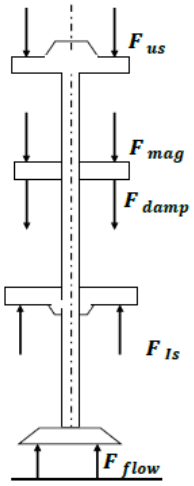

Figure 3. *Free body diagram of forces on a valve.*

2.1. Spring Forces

The upper spring force is denoted as F_{us} and the lower one as F_{ls},. These two springs have the same spring constant denoted as k_s,

For the upper spring, we can write,

$$f_{u_s} = k_s\left(c_0 + h - 4\right) = k_s\left(h_{\max} - h\right) + c_0 k_s, \tag{1}$$

And then for the lower spring,

$$f_{l_s} = k_s\left(c_0 + 4 - h\right) = k_s\left(h - h_{\max}\right) + c_0 k_s \tag{2}$$

where, c_0 is the initial compression of both springs at the equilibrium point (h). The resultant of both spring forces gives [16],

$$f_s = f_{l_s} - f_{u_s} = 2k_s\left(h_r\right), \tag{3}$$

and,

$$h_r = h - h_{\max} \tag{4}$$

where, $f_s(h)$ [N] is the elastic force exerted by springs.

2.2. Damping Force

Denoting the damping force as F_{damp}, its direction of action is in the direction of increasing h from the upper plate hence,

$$f_{damp} = -k_d\dot{h}, \tag{5}$$

where k_d is the damping coefficient.

2.3. Gaseous Flow Force

Without doubt, the combustion gases exert some force that affects the valve movement. This force is denoted as $|f_{flow}|$, at lower loads this force is small and negligible compared to the spring force during valve opening.

2.4. Electromagnetic Force

Considering an e-core geometry and flux path, and applying Gauss' law for magneto- statics [17]:

$$\oint \vec{B} \bullet dA = 0 \tag{6}$$

where B is the magnetic field and Ampere's law hence;

$$\oint \vec{H} \bullet dl = Ni \tag{7}$$

where H is the magnetic excitation, i is the current, and N the number of coil turns.

Expressing the flux in terms of the geometry, windings, material properties, air gap x, and current i for the linear (where $B=\mu H$) and magnetic saturation regions of operation. The magnetic flux is expressed as:

$$\lambda = \frac{ai}{k + x} \tag{8}$$

where a and k are constants determined by the core and armature dimensions and material properties. Integrating (8) with respect to current i gives the coil energy, which can be differentiated with respect to x (the air gap) to give the magnetic force f_{mag}:

$$f_{mag} = \frac{ai^2}{2\left(k + x\right)^2} \tag{9}$$

At higher current levels, the flux and magnetic force will vary according to (8) and (9) respectively until either the core or armature begins to saturate. At such point, an exponential form of the flux is defined that permits the characterization of the flux and magnetic force based of the B-H curve characteristic of the materials.

Hence, the equation for the voltage V_a applied across the coil then can be expressed using Kirchhoff's, Faraday's and Ohm's laws as:

$$V_a = \frac{d\lambda}{dt} + Ri, \tag{10}$$

where R is the coil resistance parameterized in terms of the e-core dimensions and wire diameter d.

Using Newton's Second Law of motion as to express the dynamics of the EMVA, we can write;

$$m\ddot{h}(t) = -k_d\dot{h}(t) - 2k_s h_r h(t) + f_{mag}(t) \tag{11}$$

Denoting $2k_s h_r = k$, we can write

$$m\ddot{h}(t) + k_d \dot{h}(t) + kh(t) = f_{mag}(t) \quad (12)$$

where m=141g, valve stroke=8mm, f_{mag} =1.8N and k_s=60N/mm, k_d=0.002s/m and h_r = 4mm (12) is re-written as;

$$0.141\ddot{h}(t) + 0.002\dot{h}(t) + 0.48h(t) = 1.8f(t) \quad (13)$$

Considering zero initial condition for all states in (13), and taking the Laplace transform of both sides of (13) gives

$$0.14s^2 H(s) + 0.002sH(s) + 0.48H(s) = 1.8F(s) \quad (14)$$

$$\left(0.14s^2 + 0.002s + 0.48\right) H(s) = 1.8F(s) \quad (15)$$

Thus, the transfer function of (15) is given as

$$G(s) = \frac{H(s)}{F(s)} = \frac{1.8}{0.14s^2 + 0.002s + 0.48} \quad (16)$$

The roots or eigenvalues of (16) are given as

$$eigenvalues = \begin{bmatrix} -0.0071 + 1.8516i \\ -0.0071 - 1.8516i \end{bmatrix} \quad (17)$$

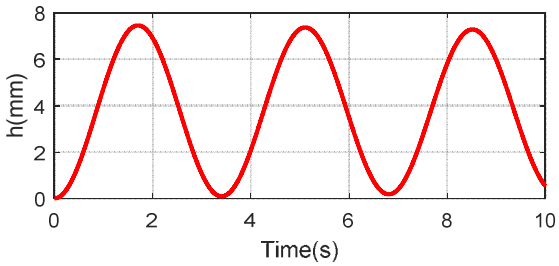

Figure 4. *Open-loop step response of the camless system.*

The basic operation requirement for the camless system is to move the valve from it's resting position to one end of the valve stroke in as short a time as possible [18]. For the camless system dynamics, it is desired that the valve lift trajectory in figure 4 stays longer (dwells) at the fully-opened-position (8mm). To achieve this feat, a form of control needs to be incorporated to the system dynamics.

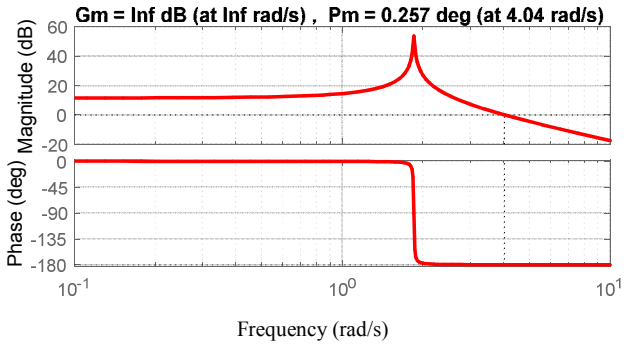

Figure 5. *Open loop Bode plot of the camless transfer function.*

3. Control Design for the Camless system Using PID

To control the dynamic system in (16), a control scheme needs to be selected. Here, we choose a set-point tracking scheme, tracking an impulse signal as depicted in Fig. 6.

3.1. Proportional Integral Derivative (PID) Control

A great number of industrial control applications are based on the PID control algorithm. The objective of this control algorithm is to make the error signal, i.e., the difference between the reference signal and the measured signal, as small as possible (go to zero with time). Mathematically, it is expressed as

$$\lim_{t\to\infty} e = \lim_{t\to\infty} r - y \to 0 \quad (18)$$

where, r is the reference signal and y is the measured signal from the sensor.

The PID control algorithm is described as:

$$\eta = K_p e(t) + K_i \int_0^t e(\tau) d\tau + K_d \frac{d}{dt} e(t), \quad (19)$$

where K_p, K_i and K_d represent proportional, integral and derivative gains respectively, and η is the input signals [19].

3.2. PID Controller Design and Simulation in MATLAB/Simulink

To design and simulate a PID controller in MATLAB/Simulink with set-point tracking scheme, Figure 6 was realized. An impulse signal was created using two *step* blocks, this served as the input to the closed-loop system. Simulation results are shown in figure 7.

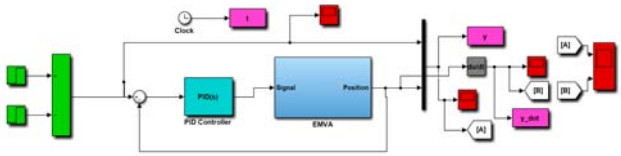

Figure 6. *Simulink model for PID control for the camless system.*

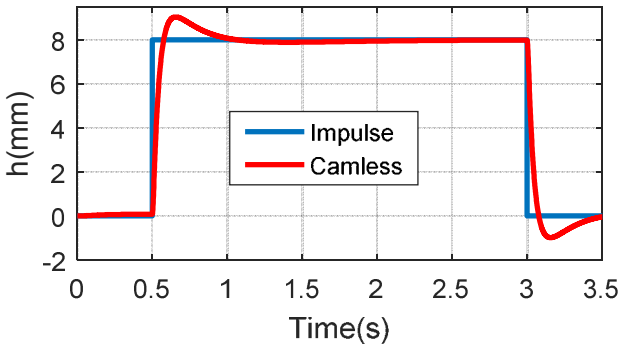

Figure 7. *Theoretical displacement profile for the camless system.*

The h and t variables that gave the result in Fig. 7 were imported into CF Toolbox of MATLAB R2016a [20]. In the CF Toolbox, we realized our theoretical model for the camless actuating system as;

$$h(t)=\sum_{n=1}^{5}\alpha\cdot a_n\sin\left(\beta\cdot b_n t+c_n\right), \qquad (20)$$

where, α = 1, β = 560, with coefficients as a_1=5.129, b_1=0.3745, c_1=0.9642, a_2=1.829, b_2=3.753, c_2=-1.895, a_3=1.202, b_3=6.322, c_3=2.896, a_4=3.959, b_4=1.37, c_4=5.43, a_5=0.8441, b_5= 8.837, c_5=1.573

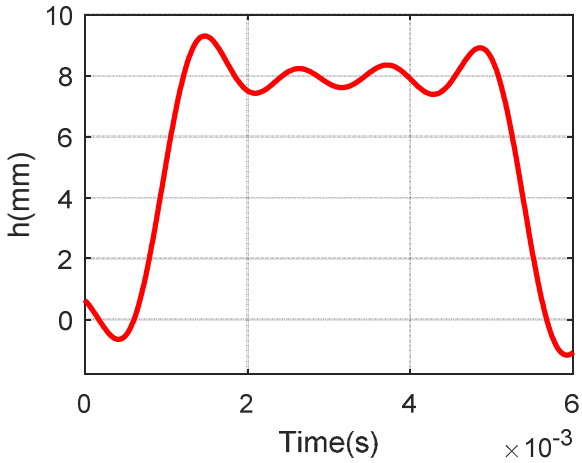

Figure 8. *Theoretical lift model for the camless system.*

4. Experimental Data Modelling for the Camless System

It is possible to get a mathematical model from experimental data of lift with time. This feat can be easily accomplished with the help of statistical curve fitting methods available. In MATLAB, the CF Toolbox *app* does curve fitting of data with relative easy.

Curve Fitting Toolbox™ provides an app and functions for fitting curves and surfaces to data. The toolbox lets you perform exploratory data analysis, pre-process and post-process data, compare candidate models, and remove outliers. You can conduct regression analysis using the library of linear and nonlinear models provided or specify your own custom equations. The library provides optimized solver parameters and starting conditions to improve the quality of your fits. The toolbox also supports nonparametric modelling techniques, such as splines, interpolation, and smoothing.

After creating a fit, you can apply a variety of post-processing methods for plotting, interpolation, and extrapolation; estimating confidence intervals; and calculating integrals and derivatives.

4.1. Goodness-of-Fit Statistics

After using graphical methods to evaluate the goodness of fit, we examined the goodness-of-fit statistics for the selection of our model. The goodness-of-fit statistics helped in determining how well the model fits the data. Such used in this study are:

a. SSE is the sum of squares due to error of the fit. A value closer to zero indicates a fit that is more useful for prediction.
b. R-square is the square of the correlation between the response values and the predicted response values. A value closer to 1 indicates that a greater proportion of variance is accounted for by the model.
c. DFE is the degree of freedom in the error.
d. Adj R-sq is the degrees of freedom adjusted R-square. A value closer to 1 indicates a better fit.
e. RMSE is the root mean squared error or standard error. A value closer to 0 indicates a fit that is more useful for prediction.
f. Number of *Coeff* is the number of coefficients in the model. When you have several fits with similar goodness-of-fit statistics, look for the smallest number of coefficients to help decide which fit is best. You must trade off the number of coefficients against the goodness of fit indicated by the statistics to avoid over-fitting.

4.2. Modelling the Experimental Camless Lift Profile

The experimental camless system data in Table 1[21], was imported into MATLAB and with CF Toolbox *app* and (21) was realized.

Table 1. *Experimental data for camless system.*

Lift(mm)	0.0	0.5	1	1.5	2.0	2.5	3.0	3.5	4.0	4.5	5.0	5.5	6.0	6.5	7.0	7.5	8.0	8.0	8.0
Time(ms)	0.0	5.5	6.9	7.8	8.5	9.2	10.0	10.5	11.4	11.8	12.2	12.6	13.5	14.0	14.5	15.9	18.0	20.0	22.0

8.0	8.0	8.0	8.0	8.0	8.0	8.0	8.0	7.5	7.0	6.5	6.0	5.5	4.5	4.0	3.5	3.0	2.5	2.0
24.0	26.0	28.0	30.0	32.0	34.0	36.0	39.0	42.5	43.5	44.2	44.8	45.2	45.6	46.4	46.9	47.5	48.0	48.5

1.5	1.0	0.5	0.0
49.0	49.5	50.5	53.0

$$h(t)=\sum_{n=1}^{7}\alpha\cdot a_n\sin\left(\beta\cdot b_n t+c_n\right) \tag{21}$$

where, a_1=8.578, b_1=57.27, c_1=-0.08096, a_2=0.2499, b_2=184.9, c_2=-3.82, a_3=1.302, b_3=285.5, c_3=-3.472, a_4=20.14, b_4=421.7, c_4=3.47, a_4=20.14, b_4=421.7, c_4=3.47, a_5=0.09739, b_5=667.4, c_5=3.771, a_6=20.05, b_6=422.4, c_6=0.3376, a_7=0.04353, b_7=891.9, c_7=0.7344.

Varying α and β arbitrarily in (21), we obtained figure 9. Combined plot of the experimental and theoretical lift models for h = 8mm and t = 6x10^{-3} s, is shown in figure 10.

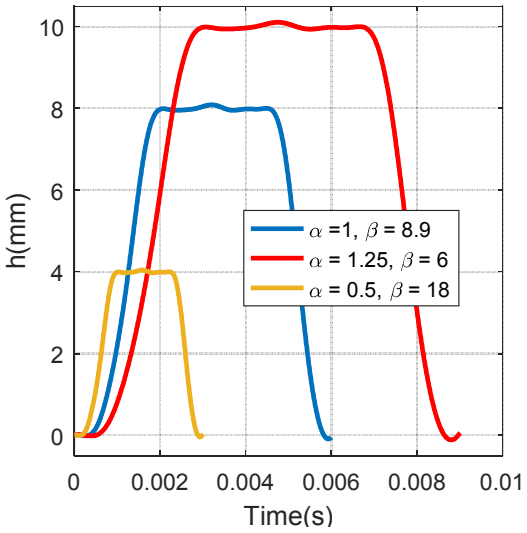

Figure 9. *Experimental lift model for camless system.*

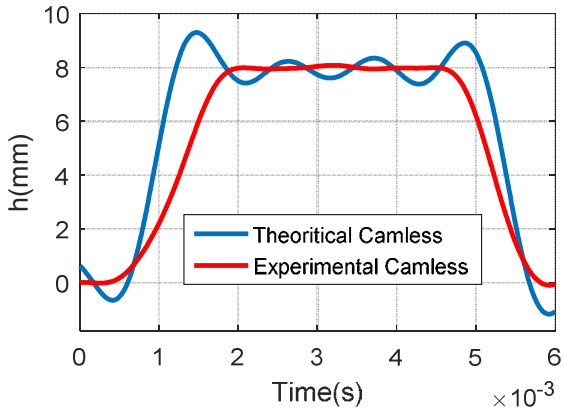

Figure 10. *Theoretical and experimental lift profile for the camless system.*

5. The Cam System

A cam system consists of four elements: cam, follower system, and drive. Cam system may be designed in variety of physical forms. The first step when designing a cam actuating system is to formulate a mathematical function to be used to define the motion of the follower. If the function of a cam is simply to move a follower through a definite displacement in a prescribed time, design requirements usually can be satisfied by some basic curves.

5.1. Theoretical Cam Actuating System

The Basic Curves methods of design are widely in use, which are primarily of two classes: simple polynomial and trigonometric. The simple polynomial curves include the constant velocity or straight line, the constant acceleration or parabolic and the cubic curves. The trigonometric curves include the elliptical, cycloidal, harmonic and double harmonic [22].

The Harmonic lift profile is expressed mathematical as given in (22). In literature, this profile is that of crankshaft angle against the piston displacement (h) in the engine cylinder.

$$\begin{aligned} h_{rise}&=\frac{h}{2}\left\{1-\cos\left(\pi\left(\frac{\theta}{\beta}\right)\right)\right\},\\ h_{fall}&=\frac{h}{2}\left\{1+\cos\left(\pi\left(\frac{\theta}{\beta}\right)\right)\right\}, \end{aligned} \tag{22}$$

where, θ is cam angle of rotation and β is cam angle for rise in h.

To obtain a common means of comparison with the camless system in this study, the need to convert the crankshaft angular displacement to a function of time is necessary. Hence, we can write;

$$t=\frac{\theta(rad)}{\omega(rad/\sec)}, \tag{23}$$

where, ω is the engine speed. We can now re-write (22) as;

$$\begin{aligned} h_{rise}&=\frac{h}{2}\left\{1-\cos\left(\pi\left(\frac{t\omega}{\beta}\right)\right)\right\},\\ h_{fall}&=\frac{h}{2}\left\{1+\cos\left(\pi\left(\frac{t\omega}{\beta}\right)\right)\right\}, \end{aligned} \tag{24}$$

A typical theoretical lift profile based on (24) can be depicted for ω = 3294.51rpm (345rad/s) as shown in figure 11

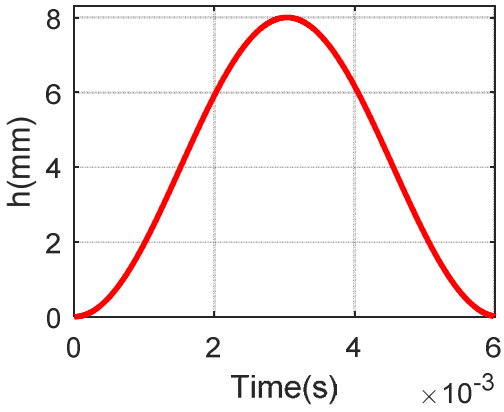

Figure 11. *Theoretical lift profile for cam system.*

5.2. Modeling the Experimental Cam Lift Profile

From experimental results [23], Table 2 was imported into the interactive CF Toolbox *app* of MATLAB 2016a was also used to get (25).

Table 2. *Experimental data for cam actuation system.*

Lift(mm)	0	0.1	0.2	0.4	0.5	0.6	0.8	1.0	1.5	2.0	2.5	3.0	3.5	4.0	4.5	5.0	5.5	6.0	6.2	6.4	6.6
Time(ms)	0	0.04	0.11	1.5	1.6	1.8	2.0	2.3	2.76	3.16	3.5	3.82	4.2	4.4	4.78	5.08	5.44	6.0	6.2	6.48	6.8

6.8	6.6	6.4	6.2	6.0	5.5	5.0	4.5	4.0	3.5	3.0	2.5	2.0	1.5	1.0	0.8	0.6	0.4	0.2	0.1
7.6	8.6	8.98	9.3	9.5	10	10.4	10.8	11.1	11.4	11.8	12.1	12.4	12.8	13.2	13.5	13.8	14.0	14.4	14.7

$$h(t)=\sum_{n=1}^{2}\alpha\cdot a_n\sin\left(\beta\cdot b_n t+c_n\right) \tag{25}$$

where, a_1=3.53, b_1=24.82, c_1=1.404, a_2=3.393, b_2=433.9, c_2=4.48.

Varying α and β in (25) can give different h and t for a complete duty circle, this is illustrated in figure 12.

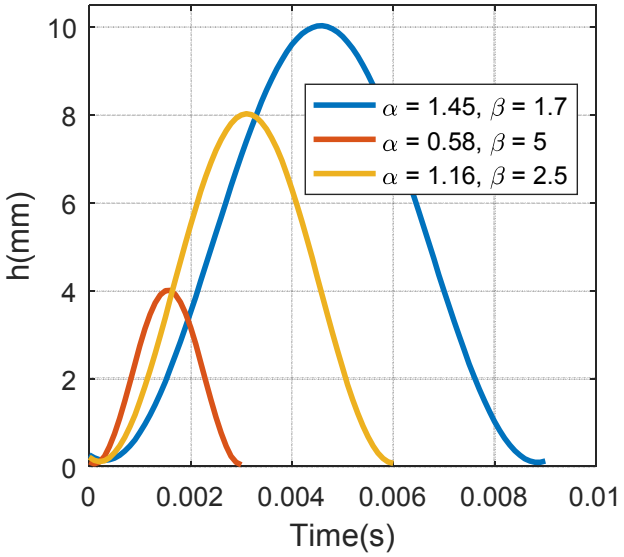

Figure 12. *Lift profile for the cam actuating system.*

Combining the theoretical and experiment lift profiles of the cam system, gave the plot in figure 13.

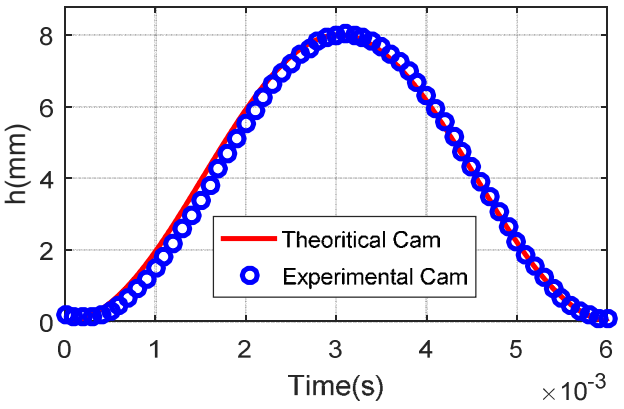

Figure 13. *Theoretical and experimental lift profile for cam system.*

6. Comparative Analysis Between Cam and Camless System

The intake system of an internal combustion engine (cam or camless) consists of the air filter, carburettor, the throttle plate, intake manifold, intake port, and intake valve. These restrict the amount of air which an engine of a given displacement can induct. The parameter used to measure the effectiveness of an engine's induction process is the volumetric efficiency [24].

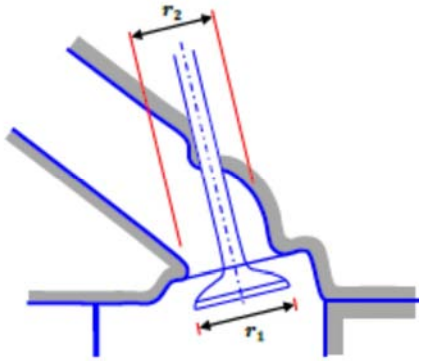

Figure 14. *Intake system of an Internal Combustion engine.*

6.1. Volumetric Efficiency

The power output of an engine depends directly on the amount of charge that can be inducted in the cylinder. This is often referred to as the breathing capacity of the engine, and is expressed quantitatively as volumetric efficiency.

Several definitions for Spark Ignition (SI) engines volumetric efficiency are given in literature. They refer to the entire intake system, comprising of air filter, inlet tract, throttle valve, intake runners, manifold and intake valve or just specific portions. The basic principles are referring to air-fuel mixture mass retention inside the cylinder at the end of the intake process or just the mass of air [25]. If the mass of air retention inside the cylinder is considered, volumetric efficiency is defined as,

$$\eta_v=\frac{n_c\dot{m}_a}{\rho_{air}v_d N}, \tag{26}$$

where, ρ_{air} is the density of air (kgm^{-3}), v_d is the displaced volume (m^3) and N is the engine speed (revolution per minutes), and n_c number of revolutions per cycle.

The mass flow rate of air in (26), has the following expression

$$\dot{m}_a = \rho_{air} v_a A, \tag{27}$$

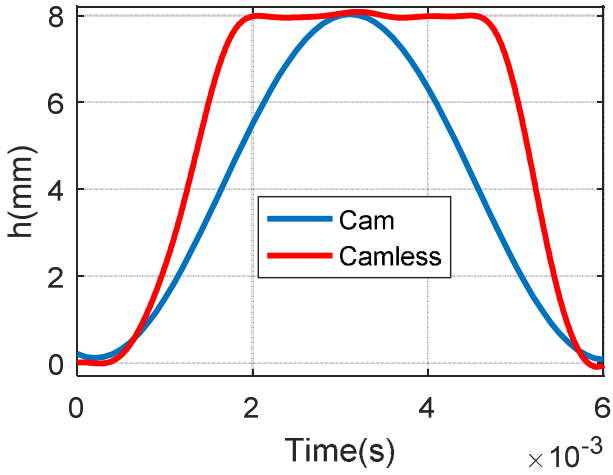

Figure 15. *Cam and Camless lift profile.*

where, v_a is the velocity of suction air and A is the area under the lift curve of both cam and camless engines as depicted in figure 15 [26]. Hence, for a four-stroke engine we can re-write (26) as;

$$\eta_v = \frac{2 v_a A}{v_d N}, \tag{28}$$

6.2. Computing Volumetric Efficiencies for Both Systems

For the velocity of flow through the inlet manifold of both systems, flow through bent duct is considered [27]. This we applied to the arrangement in Fig. 14, and the following holds:

$$p_2 - p_1 = \rho_w H_2 O g \Delta h, \tag{29}$$

where Δh = 40mm H_2O, air at STP and taking the density of water $\rho_w = 999 kg/m^3$.

Applying Euler's n component equation across the flow-stream, it can be shown that the velocity of the air into the cylinder through the manifold is expressed as

$$v_a = \left[\frac{\rho_w H_2 o g \Delta h}{\rho_a \ln(r_2 / r_1)} \right]^{1/2} \tag{30}$$

Taking $r_1 = 20mm$ and $r_2 = 21mm$ and substituting this values into (30) we have;

$$v_a = \left[\frac{999 \times 0.04 \times 9.81}{1.23 \times \ln(0.021/0.02)} \right]^{1/2} = 80.82 m/s. \tag{31}$$

Let the efficiencies of the cam and camless systems be denoted as η_c and η_{cl} respectively, we can compute both efficiencies as follows:

$$\eta_c = \frac{2 \rho_a v_a A_c}{\rho_a v_d N} \tag{32}$$

$$\eta_{cl} = \frac{2 \rho_a v_a A_{cl}}{\rho_a v_d N} \tag{33}$$

where, A_c and A_{cl} are the area under the cuvre for cam and camless engines respectively. From Fig. 15, the associated area under the curve were computed using the MATLAB command *trapz(x,y)*. Volumetric efficiencies were computed for speed values of 1000rpm to 3000rpm and graphically depicted in figure 16.

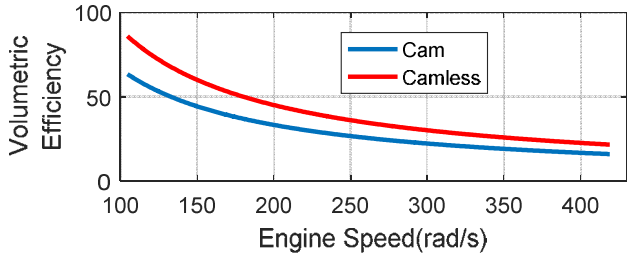

Figure 16. *Engine speed against volumetric efficiency for Cam and Camless system.*

7. Discussion of Results

The camless system eigenvalues in (17) suggests that the system dynamics is stable but oscillatory. This was corroborated by open-loop simulation result in figure 4. Also, the bode plot of the open loop system in figure 5 depicts a weak stability (Phase Margin of 0.257 at 4.04 rad/s). This is in agreement with the small magnitude of the real part of (17).

The transfer function in (16) needs to be controlled such that when it reaches the fully-open position, via a transition mode, it should dwell for some time (holding mode) before it begins to initiate the movement to attain the fully closed position (transition mode). As such, an impulse signal is generated as the input force and a PID controller was designed to track the impulse signal. Hence, a set-point control tracking scheme in MATLAB/Simulink as shown in figure 6 was designed. The PID controller has the following characteristics in Table 3. These controller gains (P, I and D) are the optimized values gotten after using the *PID controller block* to tune the system dynamics. This automated process makes MATLAB/Simulink (R2016a) very attractive for PID control design.

Table 3. *PID Controller properties.*

P	I	D	N	t_r (s)	t_r (s)	PO (%)	GM(db)	PM
2.3	1.3	1	1530	0.1s	3.7	7.3	Inf	80^0

From Table 3, the *time response characteristics* of *rise time* (t_r), *settling time* (t_s) and *percentage overshoot* (PO), are given for the optimised controller. The *phase margin* (PM) of the closed-loop system is greater than that of the open-loop system and is at 13.4 rad/s. While the *gain margin* (GM) is at

infinity (Inf), at a frequency of infinity rad/s. This implies robust stability for the closed-system.

The first stage for the realisation of our theoretical profile for the camless actuating system is depicted in figure 7. We then used the CF Toolbox of MATLAB R2016a to get a mathematical model for this theoretical lift profile. Thus, we present our novel theoretical mathematical model for the camless system as given in (20). This model served as the primary choice for curve-fitting the experimental data in Table 1.

The novel model for the camless lift profile is presented in (21). This model has the ability to depict different engine lift profiles. This capability can be achieved by randomly varying α and β until the desired trend is obtained. Typical examples are shown in figure 9.

Without doubt the experimental camless model gives us a better profile compared with it theoretical counterpart as seen in figure 10. This is inferred from both trends in figure 10 (between 0.0015s-0.005s, oscillations are not desired).

For effective comparison with the cam system, we also developed a novel mathematical model for the lift profile of the cam system, as presented in (25). This novel model for the cam lift profile has similar advantage with that of the novel camless lift profile; h and t can be varied by varying the values of α and β as shown in figure 12.

It is pertinent to note that both the theoretical and experimental lift profiles for the cam system are almost the same as seen in figure 13.

To compare camless and cam valve actuating systems, we used volumetric efficiency. The definition considered here uses mass of air retention inside the cylinder. The result is as shown in Fig. 16; the system with the largest area for a specific height (h) and time (t) will be more efficient. The camless system will always have more air retention due to larger area compare to the cam system. This makes the former better than the later at all engine speeds.

8. Conclusion

Two *sum-of-sine* mathematical equations were used to describe the lift profile of camless (EMVA) and cam valve actuating systems of Internal Combustion engines. These were achieved basically by curve-fitting their respective experimental data in MATLAB using Curve Fitting Toolbox. The mathematical equations realized in this study have the advantage of being adaptable with different engine valve stroke and timing. Volumetric efficiency computed at different engine speeds for both the camless and the cam system reveals that the former is more efficient than the later.

References

[1] V. Giglio et al (2001). Preliminary Experiences in the Design of an Electromechanical Valve Actuator. SAE Technical Paper, no. 24-0016.

[2] K. Nagaya et al (2006). Valve Timing and Valve Lift Control Mechanism for Engines. Mechatronics, 16(2):121–129.

[3] T. G. Leone et al (1996). Comparison of Variable Camshaft Timing Strategies at Part Load. SAE Technical Paper, no. 960584.

[4] R. Flierl et al (2006). Improvements to a four cylinder gasoline engine through the fully variable valve lift and timing system univalve. SAE Technical Paper, no. 01-0223.

[5] R. A. Stein et al (1995). A variable Camshaft Timing Strategy for Improved Fuel Economy and Emissions. SAE Technical Paper, no. 950975.

[6] M. M. Schechter and M. B. Levin (1996). Camless engine. SAE Technical Paper, no. 960581.

[7] M. S. Ashhab et al (1998). Control for a Robust Un-throttled Operation. SAE Technical Paper, no. 981031.

[8] R. Alzate et al (2007). Experimental and numerical verification of bifurcations and chaos in cam-follower impacting systems. Nonlinear Dynamics, 50(3):409–429.

[9] SAE (2008). Variable Valve Optimization. SP-2174. SAE International,. ISBN 978-0-7680-2016-8.

[10] A. di Gaeta et al (2010) Experimental Investigation of a Double Magnet EMVA at Key-On engine: A Mechanical Resonance Based Control Strategy. SAE International Journal of Engines, 3(2):352–372.

[11] C. David et al (2008). Fully Flexible Electromagnetic Valve Actuator: Design, Modelling, and Measurements," SAE paper no. 01-1350.

[12] Al. Williams (2002), Microcontroller projects using the Basic Stamp (2nd ed.), Focal press P.344 ISBN 978-1-57820-101-3

[13] C. Gunselmann and J. Melbert (2004). Soft-landing Control for Sensor-less Electromagnetical Spring-Mass Actuators. In Proc. of Second International Conference on Power Electronics, Machines and Drives (PEMD), volume 2, pages 715–718.

[14] Tai and T. C. Tsao (2003). Control of an electromechanical actuator for camless engines. In In Proc. of the American Control Conference, pages 3113–3118, Denver, Colorado.

[15] R. R. Chladny and Charles R. Koch (2008). Flatness-based tracking of an electromechanical variable valve timing actuator with disturbance observer feedforward compensation. IEEE Transactions on Control Systems Technology, 16(4):652–663.

[16] C. H. Velasco (2011). Modelling, Analysis, Control and Experimental Validation of Electromechanical Valve Actuators in Automotive Systems. PhD Thesis, Department of Systems and Computer Engineering Faculty of Engineering UNIVERSITY OF NAPLES FEDERICO II Naples, Italy.

[17] J. L. Chukwunek et al (2013). Modelling of Electromechanical Control of Camless Internal Combustion Engine Valve Actuator. International Journal of Science and Engineering Investigations, ISSN: 2251-8843.

[18] C. Puchalsy et al (2015). Modelica Application for Camless Engine Valve Development. 2nd Internatioanl Modelica Conference, Proceedings, pp 77-86.

[19] K. J. Astrom, Tore Hagglund (2006). Advanced PID Control ISBN 1-55617-942-1

[20] The MathWorks, Inc. (2001-2016). Curve Fitting ToolboxTM User's Guide R2016a.

[21] Parlikar et al (2005). Design and Experimental Implementation of an Electromagnetic Engine Valve Drive. IEEE/ASME Transactions on Mechatronics 10, no. 5: 482–494. http://dx.doi.org/10.1109/TMECH.2005.856221.

[22] H. A. Rothbart (2004). Cam Design Handbook. McGraw-Hill Handbook, ISBN 0-07-137757-3.

[23] D. Cope and A. Wright (2015). Engineering Matters Inc. 375 Elliot Street, Suit 130K, Newton, MA 02464. http://www.engineeringmatters.com/index.php

[24] R. Ebrahimi et al (2010). Performance of an Otto Engine with Volumetric Efficiency. Journal of American Science 2010; 6(3):27-31, ISSN: 1545-1003.

[25] A. Irimescu (2010). Study of Volumetric Efficiency for Spark Ignition Engines Using Alternative Fuels. ANUL XVII, ISSN 1453-7397.

[26] B. A. Paden et al (2015). Modeling and Control of an Electromagnetic Variable Valve Actuation System. IEEE/ASME Transactions on Mechatronics, Vol. 20, No. 6, 1083-4435.

[27] P. J. Pritchard (2011). Introduction to Fluid Mechanics. ISBN-13 9780470547557.